A Soft Approach to Convey Vibrotactile Feedback in Wearables Through Mechanical Hysteresis

Nathaniel Fino, Student Member, IEEE, Zane A. Zook, Student Member, IEEE, Barclay Jumet, Student Member, IEEE, Daniel J. Preston, Member, IEEE, Marcia K. O'Malley, Fellow, IEEE

Abstract-Vibration is ubiquitous as a mode of haptic communication, and is used widely in handheld devices to convey events and notifications. The miniaturization of electromechanical actuators that are used to generate these vibrations has enabled designers to embed such actuators in wearable devices, conveying vibration at the wrist and other locations on the body. However, the rigid housings of these actuators mean that such wearables cannot be fully soft and compliant at the interface with the user. Fluidic textile-based wearables offer an alternative mechanism for haptic feedback in a fabric-like form factor. To our knowledge, fluidically driven vibrotactile feedback has not been demonstrated in a wearable device without the use of valves, which can only enable low-frequency vibration cues and detract from wearability due to their rigid structure. We introduce a soft vibrotactile wearable, made of textile and elastomer, capable of rendering high-frequency vibration. We describe our design and fabrication methods and the mechanism of vibration, which is realized by controlling inlet pressure and harnessing a mechanical hysteresis. We demonstrate that the frequency and amplitude of vibration produced by our device can be varied based on changes in the input pressure, with 0.3 to 1.4 bar producing vibrations that range between 160 and 260 Hz at 13 to 38 g, the acceleration due to gravity. Our design allows for controllable vibrotactile feedback that is comparable in frequency and outperforms in amplitude relative to electromechanical actuators, yet has the compliance and conformity of fully soft wearable devices.

I. INTRODUCTION

Vibration is one of the most important and ubiquitous modes of haptic feedback, most notably in mobile and wearable devices, and has been used to enhance user experiences across a wide range of applications [1]. Vibrotactile feedback has become common due to the proliferation of low-cost actuators that can generate vibration. Haptic vibrations are commonly delivered to users via small actuators known as vibrotactors, available in a variety of forms, including eccentric rotating mass (ERM) actuators, linear resonant actuators (LRA), voice coil actuators, and piezo actuators. Arrays of these low-cost actuators can be combined into wearable devices (see, for example, [2]–[5]). Despite their widespread adoption, one of the primary drawbacks of these electromechanical actuators is that they are comprised of

*This material is based upon work supported by the National Science Foundation (NSF) under Grants CMMI-1830146 and CMMI-2144809 and the NSF Graduate Research Fellowship Program under Grant No. 1842494.

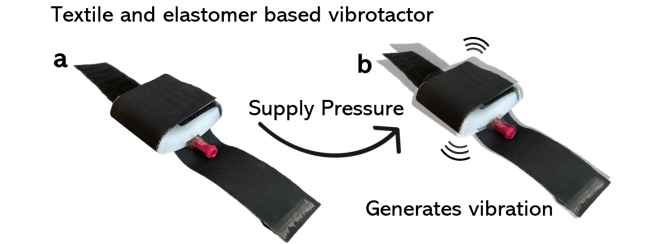


Fig. 1. Our textile- and elastomer-based vibrotactile wearable is designed to be fully compliant. The vibration effect is controlled by varying inlet pressure. (a) When unpressured, the device is compliant and passive. (b) When pressurized, the mechanism generates vibration at frequencies comparable to those realized with electromechanical vibration actuators.

rigid components, which reduces the comfort and wearability of the systems in which they are embedded.

Soft textile-based wearable devices offer an alternative to rigid electromechanical systems. They are fully compliant, washable, and allow for integration into clothing [6]. Still, these soft devices have limitations. Some must be tethered for control, adding bulk, weight, cost, and complexity [7]-[9]. The haptic cues generated by these wearables are also primarily low-frequency in nature, since the pneumatic actuation scheme must rely on opening and closing valves to vary pressure, which is inherently bandwidth-limited. Others require the use of integrated fluidic logic, which has coarser control compared to electronic systems [10]-[13]. Wearable haptic devices made with dielectric elastomer actuators (DEAs) [14] have been proposed for the arm [15] and fingertip [16], and convey vibration feedback at higher frequencies than achievable with textile-based systems. DEA-based wearables, while appealing for their low-power actuation, require large voltages to actuate, and generally do not transmit large forces to the user. Further, they are designed to exhibit a specific resonant frequency that constrains the frequency range of vibration cues that users can experience.

Recently, researchers have demonstrated the use of soft valves in soft robotic systems that self-actuate or kink at set mechanical initial conditions [17]. One method of achieving self-actuation is through hysteresis. In this context, the flexible materials snap from open to closed as pressure is released and the band is allowed to return to its biased state. A differing value of internal pressure is created from the input to the output, altering the physical state of the system and generating oscillation. Van Laake et al. used this process to create a fluidic relaxation oscillator [18] that used fluid

N. Fino, Z. Zook, and M. K. O'Malley represent the Mechatronics and Haptic Interfaces Lab, Department of Mechanical Engineering, Rice University, Houston, TX, 77005. $\{nwf2, zaz2, omalleym\}$ @rice.edu

B. Jumet and D.J. Preston represent the PI Lab, Department of Mechanical Engineering, Rice University, Houston, TX, 77005. {barclay.jumet, djp}@rice.edu

flow to control the motion of a soft robot at frequencies of 0.3 to 17 Hz. Soft wearable devices that leverage mechanical hysteresis in this way have the potential to create high-frequency vibrations without the need for electromechanical actuators or controlled valves [11], [17]–[20].

In this work, we introduce a soft wearable vibrotactor made of a silicone elastomer and heat-sealable textiles (HSTs) (Fig. 1) that is capable of producing vibration frequencies in the range of 160 to 260 Hz and amplitudes of 13 to 38 g by supplying a modulated pressure input of 0.3 to 1.4 bar. These frequencies are well-aligned with those that are sensed by mechanoreceptors in the skin [21], [22], and overlap with the range of vibrations (200-250 Hz) that have been shown to be the most salient [23]. We present the design and fabrication of our device that displays inherent hysteresis to achieve oscillatory actuation. We then experimentally demonstrate the performance of this actuation method for vibrotactile feedback, and compare our device to several electromechanical vibrotactile actuators.

II. FABRICATION PROCESS

When designing soft wearable devices, textiles are an appealing material choice due to their ubiquity in clothing and other items that directly interface with humans, given their compliance and simple, scalable methods of fabrication [24]. Furthermore, textile materials, and particularly HSTs, are low-cost, easy to employ, and can be fabricated at home using simple tools, such as a vinyl cutter and household iron [25]. Despite these advantages, researchers in soft robotics have used textiles much less often relative to other material classes [26]. We, however, leverage the advantages of HSTs for our wearable vibrotactile device. We integrate a cast silicone elastomer that maintains flexibility and conformity while providing robustness and at-home manufacturability.

A. Design

We designed the vibrotactor shape and size to be reminiscent of a watch, ensuring a well-fitting wrist-worn device. The wearable vibrotactor induces vibrations when supplied with a single, constant-pressure pneumatic input. The band comprised of HSTs serves as the foundation of the vibrotactor, housing the elastomer silicone insert and fastening around the wrist of the user. The textile band is 162 mm long, 210 mm wide, and includes a circular pouch (40-mm diameter). The integrated pouch has a 10-mm exhaust and a 5-mm inlet for a Luer lock dispensing tip. The silicone insert itself is 50 mm long and 50 mm wide with a height of 10 mm excluding the additional features. The additional features include a spherical force applicator with a diameter of 10 mm and the integrated geometry, made up of 3-mm-wide and 5-mm-high walls.

B. Materials

We selected a silicone elastomer (Ecoflex 00-30, Smoothon) to cast the vibrotactor insert and a 3D-printed thermoplastic (Hatchbox, Amazon) to create the mold. Nylon taffeta textile (FHST, Seattle Fabrics) coated with a thin film

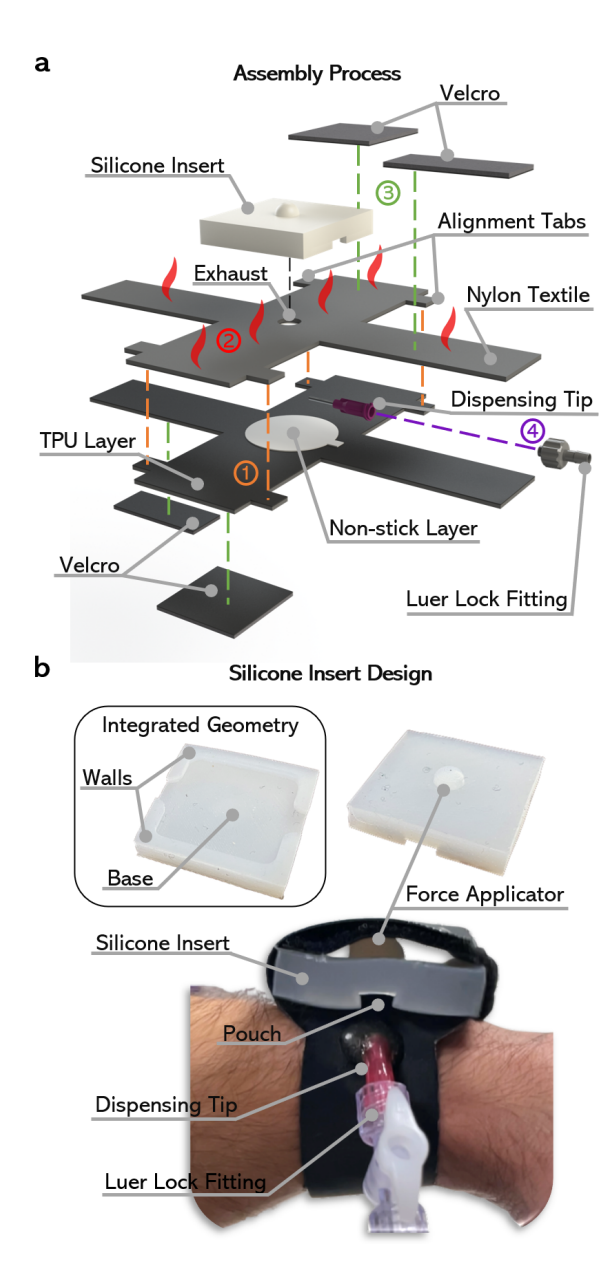


Fig. 2. The assembly process of the textile band used in this device is shown in (a). First, the alignment tabs are used to align the two halves of cut textile for heat pressing (1). Once aligned the band is thermally bonded at 195° C with an applied pressure of 345 kPa for 25 seconds (2). Once cold pressed to strengthen the layer bond and prevent wrinkling due to nonisothermal cooling, the hook and loop fasteners are attached (3). Finally, the Luer lock dispensing tip is inserted into the band and secured using epoxy (4). The silicone insert used in the fluidic vibrotactor is designed with a few key features, the integrated geometry which is comprised of the walls and base, and the force applicator as shown in (b). These key features working in concert with the textile band force the device to return to a biased resting state during actuation to facilitate mechanical hysteresis.

of thermoplastic polyurethane (TPU) constituted the band and pouch (Fig. 2). We patterned an intermediate layer, adhesive-backed paper (DL8511FS, Packzon), to prevent thermal bonding in predetermined regions so as to allow fluidic transport (through channels) and actuation (through the circular features), as shown in Fig. 2a. Soft plastic tubing connects a dispensing tip at the device's inlet (JG13-0.5HPX, Jensen Global), a quick-turn Luer lock fitting (51525K123,

McMaster-Carr), and the pressure supply. The dispensing tip is sealed to the textile band with a two-part epoxy (Plastic Bonder 50139, JB Weld) to maintain a permanent airtight seal. Finally, we attach adhesive-backed hook-and-loop fasteners (94985K35, McMaster-Carr) to the textile so that the band can secure the silicone geometry in place and be worn by the user.

C. Fabrication and Operation

The vibrotactor is manufactured using both 2D and 3D manufacturing processes (see supplemental video); we used a 3D printer (Ender 3, Creality), a vinyl cutter (Maker 3, Cricut), and a heat press (DK20SP, Digital Knight) for fabrication. We initialize the process by cutting out a square of HST and placing it on the vinyl cutter's adhesive mat with the TPU side facing up. We then place the adhesive-backed paper on top of the HST and load the adhesive mat into the vinyl cutter. Once loaded, the vinyl cutting machine cuts the exterior shape of the band, including alignment tabs (Fig. 2a). In a second cut, the machine reduces its cutting pressure to cut through only the top layer of the adhesive-backed paper, defining the geometry of the pouch and the pathway for airflow. Upon completion of the cutting process, we remove the adhesive mat from the vinyl cutter and weed the excess paper and textile. We manually orient the two halves of the textile band to each other using the alignment tabs to prevent sliding during the heat pressing process. The heat press thermally bonds the HSTs at 195 °C with an applied pressure of 345 kPa for 25 seconds. Once heat-pressed, we transfer the band to a separate cold-press to ensure stronger adhesion and to prevent the band from potential wrinkling or warping due to non-isothermal cooling. After pressing the device, we manually cut the alignment tabs from the band and insert the Luer lock dispensing tip with epoxy. Finally, the adhesivebacked hook-and-loop fasteners are attached both on the top of the textile to secure the silicone to the band, and at the bottom of the textile to fasten the band to the user. The device and its assembly process are illustrated in Fig. 2a.

Our vibrotactor operates on the principle of mechanical hysteresis (i.e., a system state-dependent behavior). Here, vibration occurs due to a mechanical bias (caused by the tensile force of the textile strap and the compliance of the elastomer) that is acted against by the inflation—and consequent pressurization—of the textile pouch. This is achieved by tightly securing the silicone over the outlet of the textile pouch (Fig. 2b). We note that the silicone insert was designed with two key features, a force applicator and integrated geometry. The force applicator provokes the system into a pressurized state through its self-centering hemispherical shape forcing the silicone to temporarily seal the outlet of the textile chamber, inducing a fluidic instability. On the other side of the silicone is the integrated geometry. The walls of the integrated geometry create a boundary of silicone around the surface of the band that separates the base of the silicone from the exhaust. The integrated geometry also forms a chamber that aids in the mechanical hysteresis (and resulting oscillatory actuation) by acting similarly to a spring as well

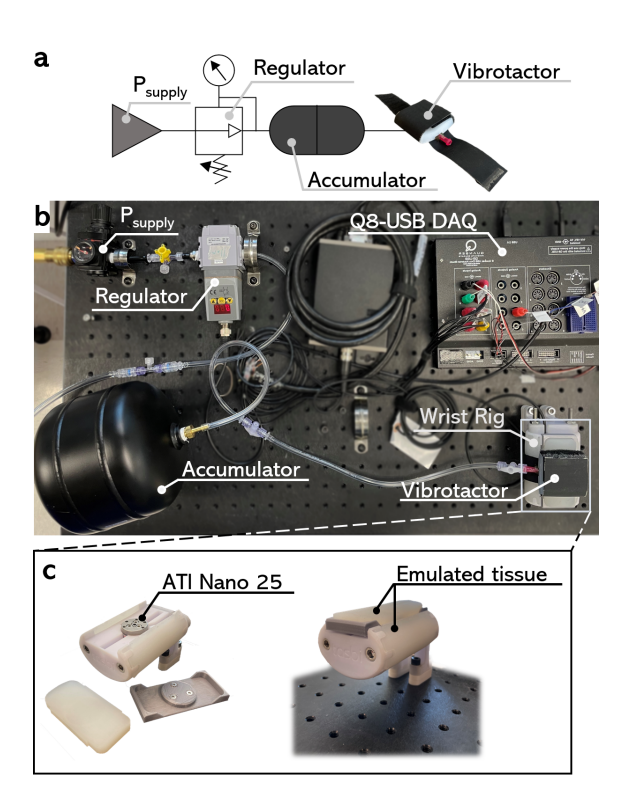


Fig. 3. An experimental test rig was used to evaluate our wearable vibrotactor. Supply pressure is provided to the soft wearable vibrotactor via a regulator and accumulator (a). The hardware system is laid out on a mechanical breadboard comprising the pressure source, regulator, accumulator, wearble device, and DAQ system (b). The wrist rig used to emulate the human wearer is comprised of a 3D-printed base to serve as the rigid skeletal structure and molded silicone to emulate human skin. An ATI Nano25 load cell housed in the wrist rig was used to measure the forces generated by the vibrotactor (c).

as allowing the textile pouch to inflate more than if the geometry were absent. In addition to fastening to a user, the textile components form a pouch that serves as a highly compliant chamber that can be inflated through pneumatic pressure. The combination of these designs creates the actuation that ultimately leads to vibration. The particular mechano-fluidic states of the device resulting from the vibration are discussed more deeply in Section III.

III. EXPERIMENTAL CHARACTERIZATION

We conducted a set of experiments to quantify the performance of our fluidic vibrotactor and benchmark it against standard electromechanical actuators for realizing vibration cues. We used an experimental test rig that emulates the human wrist shown in Fig. 3, to evaluate the vibration cues generated by our device. The wrist rig is comprised of 3D-printed parts that serve as the rigid skeletal structure of the wrist, and Ecoflex silicone molding (Ecoflex 00-30, Smoothon) to serve as the tissue and skin [2].

The testing process is initiated by supplying high pressure from the laboratory compressed air line into an electronically controlled pressure regulator (8083T1, McMaster-Carr) that regulates the air pressure from 0.1 bar to 1.5 bar in 0.1-bar intervals. An accumulator (NY-16, NYAIR) is connected downstream to the pressure regulator to act as a pneumatic

capacitor for the system. The forces generated by the vibrotactor are measured by an ATI Nano25 load cell in the instrumented wrist-shaped test rig or wrist rig, as shown in Fig. 3c. Before all trials, the vibrotactor is fastened to the wrist rig with a preload of 2 N, with the input pressure line attached to ensure consistency in test conditions across experimental trials. The load cell is then zeroed before pressurizing the vibrotactor and collecting experimental data. The data is sent via an 8-channel data acquisition (DAQ) device (Q8-USB DAQ, Quanser) for analysis. Data collection occurred during 10-s test cycles, with the last five seconds of data used in analysis to ensure steady-state behavior of the system. The raw force data collected during these five seconds were filtered using a second-order low-pass Butterworth filter with a cutoff frequency of 400 Hz and a sampling frequency of 1000 Hz. Once filtered, the time series data was then transformed to the frequency domain through a Fast Fourier Transform (FFT) to find the most prevalent frequencies. Finally, the data was rearranged using the fftshift command in Matlab to shift the zero-frequency component to the center of the frequency spectrum to properly scale the frequency values. These steps are illustrated in Fig. 4.

We compared the performance of our vibrotactor to that of commonly used electromechanical vibrotactors, namely an eccentric rotating mass (ERM) motor (306-109.002, Precision Microdrives) and a linear resonant actuator (LRA) (VG1040003D, Vybronics). We also compared our device to a solenoid valve (VT307, SMC Pneumatics), which can be used to cycle the input to fluidic actuators.

IV. RESULTS AND DISCUSSION

A. Fluidic vibrotactor performance

When pressurizing the fluidic vibrotactor, the device undergoes distinct states that result in vibration, as shown in Fig. 5a. States 1 and 6 represent the system prior to pressurization resulting in zero fluid flow $(P_{in} = 0)$. In state 2, at very low pressures ($P_{in} < 0.3$ bar), there is insufficient pressure to fully inflate the textile pouch and seal the textile against the silicone resulting in unconstrained fluid flow. In state 3, the increasing pressure inflates the band against the silicone, such that no fluid can exhaust because the breakthrough pressure needed to open the valve has not been reached (ΔP < Breakthrough). In state 4, upon reaching the breakthrough pressure ($\Delta P = Breakthrough$) the seal breaks, and the pressurized air is released, allowing the textile band to return to its biased state. (5) After the fluid is released, the band re-pressurizes, sealing itself against the silicone again until the change in pressure equals the breakthrough pressure $(\Delta P = Breakthrough)$. The process of repeating states 3–5 is responsible for the oscillatory vibration.

We varied the input pressure from 0.1 bar to 1.5 bar in 0.1-bar increments to investigate the changes in frequency and amplitude of actuation, with results shown in Fig. 5b. Inspection of the data (Fig. 4) shows that at pressures up to 0.3 bar, there is insufficient pressure to initiate vibratory behavior. When input pressures exceed 1.4 bar, the actuator remains in its open state and can no longer generate vibration

cues. We show that frequency has a negative correlation and amplitude has a positive correlation with respect to the input pressure (Fig. 5b). In other words, varying the input pressure affects the amplitude and frequency inversely as compared to a traditional ERM, where both amplitude and frequency increase with a voltage input (Fig. 5c). This relationship allows for the device to be tuned by varying the input pressure to achieve the desired frequency and amplitude.

This inverse relationship of amplitude and frequency as related to pressure is better illustrated in Fig. 5 and Fig. 4. Unlike an ERM that uses a rotating mass to create vibration, the fluidic vibrotactor opens and closes a valve shown in states 3 through 5 in Fig. 5a. The action of opening and closing the valve requires a set input pressure of $P_{in} \ge 0.3$ bar and $P_{in} \leq$ 1.4 bar. As the pressure rises to $P_{in} \geq$ 1.5 bar, the pressure becomes too great for the actuator to return to its biased state. This causes the fluidic vibrotactor to remain open, similar to what is shown in state 4. Keeping the valve open longer physically limits the frequency produced as the valve cannot close as fast as the driving signal is generating the vibratory action. This slowed frequency increases the amplitude as the valve is now being stretched open further, causing more force upon closing. This is how the fluidic vibrotactor produces an inverse relationship of frequency and amplitude compared to an ERM. This inverse relationship could prove to display a new perceptual set of cues. These cues provide higher frequencies which are more perceivable on the skin, but provide them with less amplitude. However, lower frequencies which are typically less perceivable, now provide more amplitude to a user during actuation.

B. Comparing Vibration Based Actuators

We experimentally compared the performance of our vibrotactile actuator against two electromechanical vibrotactile actuators (ERM and LRA), and solenoid-based actuation of fluidic textile-based wearables (see Table: I). We present the maximum and minimum frequencies of realized vibrations, the maximum and minimum amplitudes of vibration, and the range of vibration frequencies and amplitudes achievable with each device. Our results show that the fluidic vibrotactor designed in this work compares well against the state of the art with an amplitude range of 25 g (acceleration due to gravity) and a frequency rage of 100 Hz, surpassing that of the LRA and the solenoid. The ERM has a wider achievable frequency range, 2.4 times that of the fluidic vibrotactor. Though our proposed device has a narrower frequency range compared to ERMs, it is still within the ideal perceivable range for humans (200-250Hz) [23], [27], with a wider amplitude range during actuation. ERMs may be able to provide vibrations with larger amplitude than our device, but it is worth noting that these devices require larger masses to generate more force, and as the added mass grows so does the size and mass of the electric motor that drives it. This means for an ERM to provide greater amplitude, the actuator itself must grow in size. Depending on the physical size constraints of a given application, an ERM source of vibraiton may not be feasible. For the achievable frequency

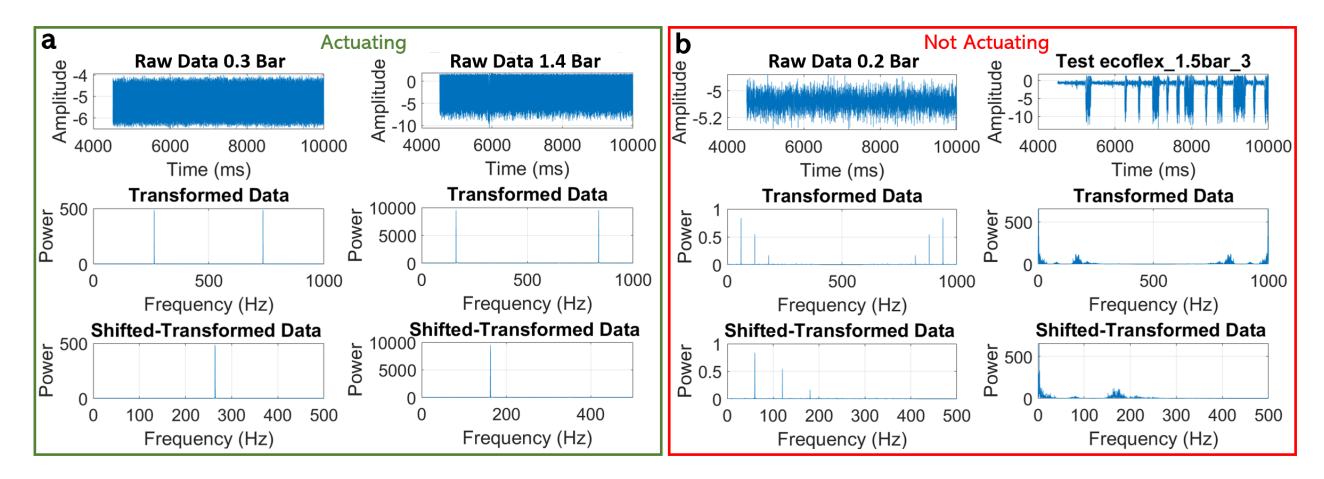


Fig. 4. We present two modes of operation of the fluidic vibrotactor. When actuating, the fluidic vibrotactor has a pressure threshold ($P_{in} \ge 0.3$ bar and $P_{in} \le 1.4$ bar) at which the device achieves its maximum frequency and bandwidth (a). Outside of this threshold, the vibrotactor will not oscillate, either due to a lack of input pressure ($P_{in} = 0$) or due to exceeded pressures ($P_{in} \ge 1.5$ bar) (b). Within each sub-plot, we show the steps of data analysis. We first present the raw data prior to filtering. Then, the data is transformed via filtering and FFT. Finally, the shifted and transformed data is rearranged (using the fftshift command in Matlab) to properly scale the frequency values.

and amplitude values of our fluidic-textile device compared to an ERM, LRA and solenoid, the fluidic vibrotactor shows promise as a standalone alternative to typical electromechanical vibrotactors. Furthermore, this device has the potential to create complex psychophysical sensations differing from that of an electromechanical actuator due to its size, inverse pressure relationship, and compliant structure.

V. CONCLUSIONS

In this paper, we present a wearable haptic feedback device designed to provide vibration cues to the user. The device is comprised of heat sealable textiles and elastomeric materials, resulting in a fully compliant device, in contrast to currently available systems that rely on electromechanical actuators like ERMs or LRAs, or controlled valves to deliver vibration

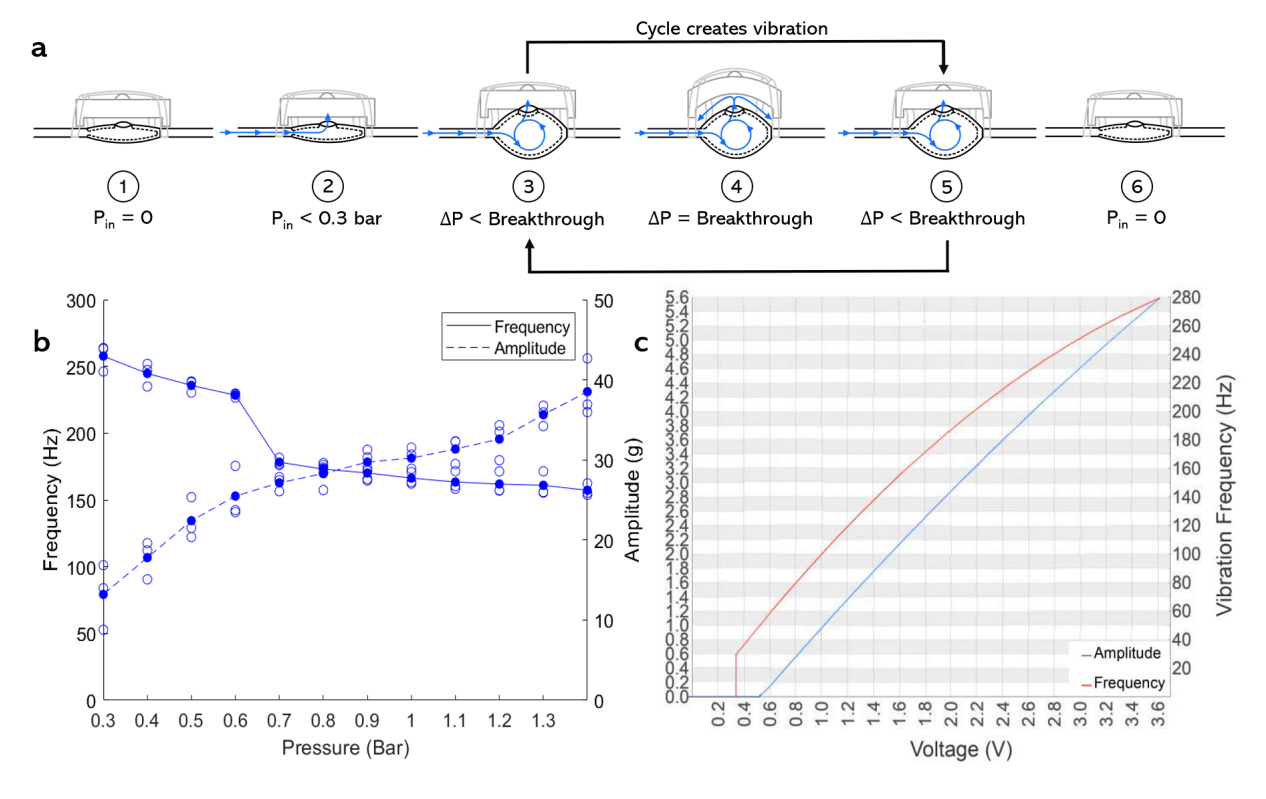


Fig. 5. The fluidic vibrotactor has six distinct states, unpressurized (1,6), under pressurized (2) and vibrating (3-5) shown in (a). When vibrating the amplitude and frequency compared to input pressure scale inversely to one another due to the device's dependence on pressure input. As the pressure increases the vibrotactor stays open longer slowing frequency but increasing amplitude (b). Unlike the vibrotactor the ERMs frequency and amplitude compared to the input voltage are scaled positively, due to the dependence of the attached offset mass on the speed of the electric motor (c) (Precision Microdrives Data Sheet Model: 306-109.002).

TABLE I
COMPARISON OF ACTUATORS

Actuators	Min Frequency (Hz)	Max Frequency (Hz)	Min Amplitude (g)	Max Amplitude (g)	Frequency Range (Hz)	Amplitude Range (g)
ERM (306-109.002)	30	270	0.6	5.4	240	4.8
LRA (VG1040003D)	100	174	0.2	2.1	74	1.9
Solenoid (VT307)	0	10	-	-	10	-
This work	160	260	13	38	100	25

cues to the wearer. The device is fabricated using low cost materials and accessible manufacturing methods including vinyl cutting and 3D-printing. The vibrations are realized through mechanical hysteresis, which is possible due to a biased orientation of the device, created by the integrated features found in the silicone insert and textile band. We demonstrated the dynamic range of the soft vibrotactor by varying the input pressure from 0.3 to 1.4 bar, which resulted in vibration frequencies between 160 and 260 Hz with amplitudes ranging from 13 to 38 g. We also show that our design exhibits an inverse relationship between frequency and amplitude compared to input pressure. This is counter to what is seen in ERM-based vibration devices, where both frequency and amplitude scale positively with input DC voltage. Looking to the future, this device could be modified to alter its frequency or amplitude through the design of differently shaped silicone inserts. These inserts could employ varying wall thicknesses or integrated geometries with the potential to produce differing frequency and amplitude ranges.

REFERENCES

- S. Choi and K. J. Kuchenbecker, "Vibrotactile display: Perception, technology, and applications," *Proceedings of the IEEE*, vol. 101, pp. 2093–2104, Sep. 2013.
- [2] E. Pezent, P. Agarwal, J. Hartcher-OrBrien, N. Colonnese, and M. K. O'Malley, "Design, control, and psychophysics of tasbi: A force-controlled multimodal haptic bracelet," *IEEE Transactions on Robotics*, vol. 38, no. 5, pp. 2962–2978, 2022.
- [3] A. S. Macklin, J. M. Yau, and M. K. O'Malley, "Evaluating the effect of stimulus duration on vibrotactile cue localizability with a tactile sleeve," *IEEE Transactions on Haptics*, vol. 14, no. 2, pp. 328–334, 2021.
- [4] C. M. Reed, H. Z. Tan, Z. D. Perez, E. C. Wilson, F. M. Severgnini, J. Jung, J. S. Martinez, Y. Jiao, A. Israr, F. Lau, et al., "A phonemicbased tactile display for speech communication," *IEEE transactions* on haptics, vol. 12, no. 1, pp. 2–17, 2018.
- [5] S. Choi and K. J. Kuchenbecker, "Vibrotactile display: Perception, technology, and applications," *Proceedings of the IEEE*, vol. 101, no. 9, pp. 2093–2104, 2013.
- [6] C. Thalman and P. Artemiadis, "A review of soft wearable robots that provide active assistance: Trends, common actuation methods, fabrication, and applications," Wearable Technologies, vol. 1, p. e3, 2020.
- [7] E. M. Young, A. H. Memar, P. Agarwal, and N. Colonnese, "Bellowband: A pneumatic wristband for delivering local pressure and vibration," in 2019 IEEE World Haptics Conference (WHC), pp. 55–60, IEEE.

- [8] M. Zhu, A. H. Memar, A. Gupta, M. Samad, P. Agarwal, Y. Visell, S. J. Keller, and N. Colonnese, "PneuSleeve: In-fabric multimodal actuation and sensing in a soft, compact, and expressive haptic sleeve," in *Proceedings of the 2020 CHI Conference on Human Factors in Computing Systems*, pp. 1–12, ACM.
- [9] B. Jumet, Z. A. Zook, D. Xu, N. Fino, A. Rajappan, M. W. Schara, J. Berning, N. Escobar, M. K. O'Malley, and D. J. Preston, "A textile-based approach to wearable haptic devices," in 2022 IEEE 5th International Conference on Soft Robotics (RoboSoft), pp. 741–746, 2022.
- [10] S. Song, S. Joshi, and J. Paik, "Cmos-inspired complementary fluidic circuits for soft robots," *Advanced Science*, vol. 8, no. 20, p. 2100924, 2021
- [11] D. J. Preston, P. Rothemund, H. J. Jiang, M. P. Nemitz, J. Rawson, Z. Suo, and G. M. Whitesides, "Digital logic for soft devices," *Proceedings of the National Academy of Sciences*, vol. 116, no. 16, pp. 7750–7759, 2019.
- [12] C. J. Decker, H. J. Jiang, M. P. Nemitz, S. E. Root, A. Rajappan, J. T. Alvarez, J. Tracz, L. Wille, D. J. Preston, and G. M. Whitesides, "Programmable soft valves for digital and analog control," *Proceedings of the National Academy of Sciences*, vol. 119, no. 40, p. e2205922119, 2022.
- [13] A. Rajappan, B. Jumet, R. A. Shveda, C. J. Decker, Z. Liu, T. F. Yap, V. Sanchez, and D. J. Preston, "Logic-enabled textiles," *Proceedings of the National Academy of Sciences*, vol. 119, no. 35, p. e2202118119, 2022.
- [14] E. Hajiesmaili and D. R. Clarke, "Dielectric elastomer actuators," Journal of Applied Physics, vol. 129, no. 15, p. 151102, 2021.
- [15] H. Zhao, A. M. Hussain, A. Israr, D. M. Vogt, M. Duduta, D. R. Clarke, and R. J. Wood, "A wearable soft haptic communicator based on dielectric elastomer actuators," *Soft robotics*, vol. 7, no. 4, pp. 451–461, 2020.
- [16] J.-H. Youn, H. Mun, and K.-U. Kyung, "A wearable soft tactile actuator with high output force for fingertip interaction," *IEEE Access*, vol. 9, pp. 30206–30215, 2021.
- [17] K. Luo, P. Rothemund, G. M. Whitesides, and Z. Suo, "Soft kink valves," *Journal of the Mechanics and Physics of Solids*, vol. 131, pp. 230–239, 2019.
- [18] L. C. van Laake, J. de Vries, S. Malek Kani, and J. T. Overvelde, "A fluidic relaxation oscillator for reprogrammable sequential actuation in soft robots," *Matter*, vol. 5, no. 9, pp. 2898–2917, 2022.
- [19] T. Park, E. Choi, C.-S. Kim, J.-O. Park, and A. Hong, "A multi-segmented soft finger using snap-through instability of a soft valve with a slit," *IEEE Robotics and Automation Letters*, vol. 7, no. 3, pp. 6990–6997, 2022.
- [20] P. Rothemund, A. Ainla, L. Belding, D. J. Preston, S. Kurihara, Z. Suo, and G. M. Whitesides, "A soft, bistable valve for autonomous control of soft actuators," *Science Robotics*, vol. 3, no. 16, p. eaar7986, 2018.
- [21] I. Hwang and S. Choi, "Perceptual space and adjective rating of sinusoidal vibrations perceived via mobile device," 2010 IEEE Haptics Symposium, pp. 1–8, 2010.
- [22] H. Z. Tan, N. I. Durlach, C. M. Reed, and W. M. Rabinowitz, "Information transmission with a multifinger tactual display," *Perception & Psychophysics*, vol. 61, pp. 993–1008, Aug. 1999.
- [23] V. B. Mountcastle, R. H. LaMotte, and G. Carli, "Detection thresholds for stimuli in humans and monkeys: comparison with threshold events in mechanoreceptive afferent nerve fibers innervating the monkey hand.," *Journal of Neurophysiology*, vol. 35, no. 1, pp. 122–136, 1972.
- [24] V. Sanchez, C. J. Walsh, and R. J. Wood, "Textile technology for soft robotic and autonomous garments," *Advanced Functional Materials*, vol. 31, no. 6, p. 2008278, 2021.
- [25] M. Schara, M. Zeng, B. Jumet, and D. J. Preston, "A low-cost wearable device for portable sequential compression therapy," *Frontiers in Robotics and AI (in press)*, 2022.
- [26] B. Jumet, M. D. Bell, V. Sanchez, and D. J. Preston, "A data-driven review of soft robotics," *Advanced Intelligent Systems*, vol. 4, no. 4, p. 2100163, 2022.
- [27] M.-H. Choi, B. Kim, H.-S. Kim, S.-Y. Gim, W.-R. Kim, and S.-C. Chung, "Perceptual threshold level for the tactile stimulation and response features of ERD/ERS-based specific indices upon changes in high-frequency vibrations," *Frontiers in Human Neuroscience*, vol. 11, p. 207, 2017.